POLITECNICO DI TORINO
Repository ISTITUZIONALE

Risk of myocardial infarction based on endothelial shear stress analysis using coronary angiography

Original
Risk of myocardial infarction based on endothelial shear stress analysis using coronary angiography / Candreva, A., Pagnoni, M., Rizzini, M.L., Mizukami, T., Gallinoro, E., Mazzi, V., Gallo, D., Meier, D., Shinke, T., Aben, J., Nagumo, S., Sonck, J., Munhoz, D., Fournier, S., Barbato, E., Heggermont, W., Cook, S., Chiastra, C., Morbiducci, U., De Bruyne, B., et al.. - In: ATHEROSCLEROSIS. - ISSN 0021-9150. - 342:(2022), pp. 28-35. [10.1016/j.atherosclerosis.2021.11.010]

Availability:
This version is available at: 11583/2972252 since: 2022-10-12T11:06:53Z

Publisher:
ELSEVIER IRELAND LTD

Published
DOI:10.1016/j.atherosclerosis.2021.11.010

Terms of use:

This article is made available under terms and conditions as specified in the corresponding bibliographic description in the repository

Publisher copyright

(Article begins on next page)

19 November 2026

Risk of Myocardial Infarction based on Endothelial Shear Stress Analysis Using Coronary Angiography

Running title: Endothelial shear stress predicts myocardial infarction.
Total word count (main text including legends to figures and tables): 3'796 words.
Number of figures and/or tables: 3 figures and 2 tables.
Number of references: 28.

Alessandro Candreva, MD[a,b], Mattia Pagnoni, MD[c], Maurizio Lodi Rizzini, MS[d], Takuya Mizukami, MD, PhD[a,e], Emanuele Gallinoro, MD[a,f], Valentina Mazzi, MS[d], Diego Gallo, PhD[d], David Meier, MD[c], Toshiro Shinke, MD,PhD[e], Jean-Paul Aben, MSc[g], Sakura Nagumo, MD[a,e], Jeroen Sonck, MD[a,h], Daniel Munhoz MD, PhD[a,h,i], Stephane Fournier, MD[c,h], Emanuele Barbato MD, PhD[a,h], Ward Heggermont, MD, PhD[a], Stephane Cook, MD[j], Claudio Chiastra, PhD[d], Umberto Morbiducci, PhD[d], Bernard De Bruyne, MD, PhD[a,c], Oliver Muller, MD, PhD[c], and Carlos Collet, MD, PhD[a*]

[a] Cardiovascular Center Aalst, OLV-Clinic, Aalst, Belgium
[b] Dept. of Cardiology, Zurich University Hospital, Zurich, Switzerland
[c] Dept. of Cardiology, Lausanne University Hospital, Lausanne, Switzerland
[d] Dept. of Mechanics, Politecnico di Torino, Turin, Italy
[e] Dept. of Cardiology, Showa University School of Medicine, Tokyo, Japan
[f] Dept. of Translational Medical Sciences, University of Campania 'Luigi Vanvitelli', Naples, Italy
[g] Pie Medical Imaging BV, Maastricht, The Netherlands
[h] Dept. of Advanced Biomedical Sciences, University of Naples Federico II, Naples, Italy
[i] Department of internal medicine, University of Campinas (Unicamp), Campinas, Brazil.
[j] Department of Cardiology, HFR Fribourg, Fribourg, Switzerland
[*] Corresponding author

Address for correspondence:
Carlos Collet Bortone, MD, PhD
Cardiovascular Center Aalst, OLV-Clinic, Aalst, Belgium.
Moorselbaan, 1654, B-9300 Aalst; Phone: +32 53 72 44 39;
e-mail: carloscollet@gmail.com

Abstract

Background and aims: Wall shear stress (WSS) has been associated with atherogenesis and plaque progression. The present study assessed the value of WSS analysis derived from conventional coronary angiography to detect lesions culprit for future myocardial infarction (MI).

Methods and Results: Three-dimensional quantitative coronary angiography (3DQCA), was used to calculate WSS and pressure drop in 80 patients. WSS descriptors were compared between 80 lesions culprit of future MI and 108 non-culprit lesions (controls). Endothelium-blood flow interaction was assessed by computational fluid dynamics (10.8±1.41 min per vessel). Median time between the baseline angiography and MI was 25.9 (21.9-29.8) months. Mean patient age was 70.3±12.7. Clinical presentation was STEMI in 35% and NSTEMI in 65%. Culprit lesions showed higher percent area stenosis (%AS), translesional vFFR difference (ΔvFFR), time-averaged WSS (TAWSS) and topological shear variation index (TSVI) compared to non-culprit lesions (p<0.05 for all). TSVI was superior to TAWSS in predicting MI (AUC-TSVI=0.77, 95%CI 0.71-0.84 vs. AUC-TAWSS=0.61, 95%CI 0.53-0.69, p<0.001). The addition of TSVI increased predictive and reclassification abilities compared to a model based on %AS and ΔvFFR (NRI=1.04, p<0.001, IDI=0.22, p<0.001).

Conclusions: A 3DQCA-based WSS analysis was feasible and can identify lesions culprit for future MI. The combination of area stenoses, pressure gradients and WSS predicted the occurrence of MI. TSVI, a novel WSS descriptor, showed strong predictive capacity to detect lesions prone to cause MI.

Highlights:

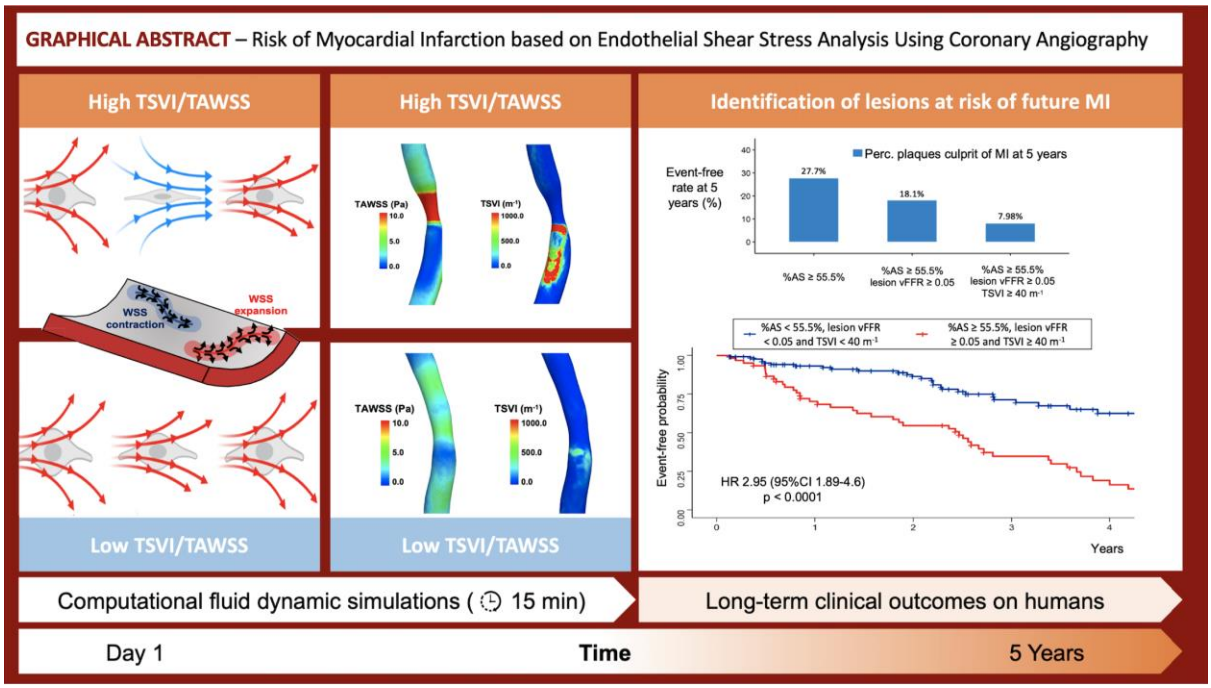
- Lesions culprit of future MI had higher area stenoses, pressure gradients, TAWSS and TSVI.
- A 3DQCA-based software provided in few minutes reliable WSS simulations.
- The novel WSS-based descriptor TSVI showed strong predictive capacity for future MI.

Keywords: Wall Shear Stress; Myocardial infarction; Computation Fluid Dynamics; Virtual Fractional Flow Reserve; Quantitative Coronary Angiography; Time-averaged Wall Shear Stress; Topological Shear Variation Index.

Abbreviations:

%AS	Percent area stenosis	MLD	Minimal lumen diameter
CABG	Coronary artery bypass graft	NCL	Non-culprit lesion
CAD	Coronary artery disease	QCA	Quantitative coronary angiography
CFD	Computational fluid dynamics	TSVI	Topological shear variation index
FCL	Future culprit lesion	vFFR	Virtual fractional flow reserve
FFR	Fractional flow reserve	WSS	Wall shear stress
MI	Myocardial infarction		

Graphical Abstract – Risk of myocardial infarction based on endothelial shear stress analysis using coronary angiography.



Shear forces acting on endothelial surface can be simulated with computational fluid dynamics-based software from conventional coronary angiograms. The variability of local contraction/expansion action exerted by shear forces along the cardiac cycle is captured by the topological shear variation index (TSVI, in m^{-1}), while the time-averaged wall shear stress (TAWSS, in Pa) describes their averaged magnitude along the cardiac cycle. Both WSS-based descriptors identified lesions culprit of myocardial infarction at 5 year, however TSVI could significantly further improve predictivity, reclassification and discriminatory capacity when added to percentage area stenosis (%AS) and translesional difference in the virtual fractional flow reserve (ΔvFFR).

Introduction

Coronary arteries – and atherosclerotic plaques – experience a variety of mechanical forces linked to plaque progression and destabilization.[1, 2] Among them, high pressure gradients across epicardial lesions have been recognized as independent predictors of myocardial infarction (MI).[3] The frictional force of the flowing blood acting on the endothelium, i.e. wall shear stress (WSS), is also a key mechanism translating hemodynamic signals to vascular biological phenomena.[4, 5] In addition, WSS has been associated with vulnerable transformation of atherosclerotic lesions: low WSS has been linked to atherosclerosis progression, whereas high WSS has been associated with platelet activation and plaque rupture.[6, 7] More recently, WSS-based descriptors able to characterize the contraction/expansion action of endothelial shear forces along the cardiac cycle were associated with vascular pathophysiological processes in coronary and extra-coronary territories.[8-10] In particular, a recent longitudinal study on swine models showed that early atherosclerotic changes in coronary arteries are associated with the endothelium shear stress contraction/expansion variability along the cardiac cycle, captured by the WSS-based quantity topological shear variation index (TSVI).[10]

The present study evaluates the efficacy of an anatomical and hemodynamic assessment based on computational fluid dynamic (CFD) simulations, obtained from conventional coronary angiography for the identification of lesions prone to cause MI within five years.

Materials and Methods

Study design

This is a case-control multicenter study including three European centers (OLV clinic, Aalst, Belgium; University of Lausanne, Switzerland; Fribourg Cantonal Hospital, Switzerland) designed to identify predictors of MI. Study protocol conforms to the ethical guidelines of the 1975 Declaration of Helsinki and has been approved by the Institution's ethics committee. Written informed consent was obtained from each patient included in the study.

Study population

Patients presenting with acute MI admitted for invasive coronary angiography were screened to identify those who (i) had a previous coronary angiography (here forth referred as baseline angiography) performed between 1 month and 5 years before the index event, (ii) had the visually identifiable mild lesion (≤ 50% visual diameter stenosis) culprit for the future MI at the baseline angiography, and (iii) had at the baseline angiography at least one additional non-culprit lesion (NCL) in at least one of the other two major epicardial vessels. Therefore, each patient served as its own control. Patient exclusion criteria were post-coronary artery bypass graft (CABG) status, MI as result of in-stent restenosis or thrombosis, MI in absence of angiographically identifiable coronary lesions, ostial lesions or lesions involving a coronary bifurcation with a side branch diameter ≥ 2 mm. In case of multiple coronary angiographies before the acute event, the latest angiography was selected for analysis.

Lesion selection (for both future culprit lesions, FCL, and NCL) was performed blinded to the information of which lesion evolved towards an MI. Subsequently, three-dimensional

geometries derived from coronary angiography of both FCL and NCL were generated for blood flow simulations.

Coronary angiography and blood flow simulations

The workflow of the study is presented in **Figure 1**. Three-dimensional quantitative coronary angiography (3DQCA) reconstructions were performed using two angiographic end-diastolic frames at least 30 degrees apart using the CAAS Workstation WSS software (Pie Medical Imaging, Maastricht, the Netherlands). Automated lumen contour detection was enabled, and manually corrected when needed. Three-dimensional coronary reconstruction included at least 20 mm proximally and 20 mm distally from the minimal lumen diameter (MLD). Using the three-dimensional coronary reconstruction, CFD simulations were carried out automatically using a finite element-based code (CAAS Workstation WSS software) to quantify WSS distribution along the cardiac cycle under resting conditions. Details on numerical settings are reported in the **Supplemental Methods**. Simulations were performed on a standard computer with processor Intel Xeon W-2123, 3.6GHz, 4 cores, RAM 16Gb.

3DQCA and the angiography-derived virtual fractional flow reserve (vFFR) were obtained using the CAAS Workstation vFFR software (Pie Medical Imaging) on the same angiographic projections selected for three-dimensional vessels reconstruction. Anatomical descriptors included percentage area stenosis (%AS), percentage diameter stenosis, minimal lumen area (MLA) and diameter, reference vessel diameter, lesion length and distance of MLA from the ostium. The distal vFFR, the translesional vFFR difference (ΔvFFR), and the absolute pressure drop in millimeters of mercury (mmHg) at the distal part of the vessel, i.e. distal pressure gradient, were extracted as detailed elsewhere.[11]

Wall shear stress descriptors

The quantitative characterization of endothelial shear forces included the following WSS-based descriptors (**Supplemental Table 1**): time-averaged wall shear stress (TAWSS), obtained by averaging the local values of WSS magnitude along the cardiac cycle (**Supplemental Figure 1**);[12] oscillatory shear index (OSI);[13] transverse WSS (transWSS);[14] TAWSS axial component ($TAWSS_{ax}$) and secondary component ($TAWSS_{sc}$);[15] relative residence time (RRT);[16] and topological shear variation index (TSVI).[8-10] The next paragraph further expands on TSVI.

Endothelial contraction/expansion regions can be mathematically identified analyzing the WSS topological skeleton, in particular through negative/positive local values of the divergence of the WSS unit vector field (DIV_{WSS}).[17] Technically, the variability of DIV_{WSS} along the cardiac cycle can be measured using the WSS-based quantity TSVI [17] (**Supplemental Figure 2** and **Supplemental Movie**), defined as the root mean square deviation of the instantaneous divergence of the unit WSS vector field with respect to its average over the cardiac cycle:

$$\mathrm{TSVI} = \left\{\frac{1}{\mathrm{T}}\int_0^{\mathrm{T}}[\mathrm{DIV_{WSS}} - \overline{\mathrm{DIV_{WSS}}}]^2\mathrm{dt}\right\}^{1/2}, \quad \text{(Eq. 1)}$$

where T is the duration of the cardiac cycle and the overbar denotes a cycle-average quantity. Theoretical and technical details on the method of analysis of the WSS topological skeleton here adopted have been exhaustively reported elsewhere.[17]

The WSS-based descriptors are presented as averaged or maximum and minimum values over three distinct vessel segments: (i) lesion, defined as the segment including the MLA and delimited proximally and distally by the intersection of the QCA diameter function line

with the interpolated reference line, (ii) an upstream segment with a length of three times the diameter of the proximal boundary of the lesion, and (iii) a downstream segment with a length of three times the diameter of the distal boundary of the lesion, to ensure a consistent spatial extent across all cases (**Supplemental Figure 3)**.

To assess reliability, CFD simulations carried out by physicians (AC) in standard clinical settings (hence denoted as 'clinical CFD') using the CAAS Workstation WSS software were tested against state-of-the-art simulations carried out by experts in computational hemodynamics (MLR, VM, DG, CCh, UM) with higher resolution and numerical robustness ('expert CFD'), as further detailed in **Supplemental Methods**. The capability of WSS-based quantities to discriminate FCL vs. NCL groups was tested for both clinical and expert CFD.

To assess the reproducibility of the WSS evaluation process, thirty coronary arteries were randomly selected and WSS simulations were repeated with the same software.

Statistical Methods

All statistical analyses were performed on a per-lesion basis to compare FCL and NCL characteristics. Continuous variables with normal distribution are presented as mean±standard deviation (SD) and non-normally distributed variables as median (inter-quartile range [IQR]). Categorical variables are presented as percentages. Chi-squared test was used for comparing categorical variables, while Student's tests (or Mann-Whitney tests as appropriate) for continuous ones. A p-value <0.05 was considered significant. The predictive capacity of QCA-, vFFR- and WSS-based descriptors was assessed using C-statistics. Receiving operator characteristic (ROC) curve were compared using the DeLong method.[18] To determine the net reclassification index (NRI) and relative integrated discrimination improvement (IDI) for each

model, continuous variables were dichotomized according to optimal cut-off values from the ROC curves. Three models were defined: the anatomical model (based on %AS) (model 1), the anatomical and pressure model (based on %AS and ΔvFFR) (model 2), and a third model based on %AS, ΔvFFR and a WSS descriptor (model 3). Time-to-event data are presented as Kaplan-Meier estimates. Anatomical and functional variables presenting a univariate relationship with future MI entered the multivariate Cox proportional-hazards regression models. Associated risk for discrete increments was assessed with odds ratio (OR) derived from binary logistic regression. WSS-based quantities reproducibility was assessed with intraclass correlation coefficients (ICC). All analyses were performed using R statistical software (R Foundation for Statistical Computing, Vienna, Austria).

Results

Patient selection

From January 2008 to December 2019, 6885 patients underwent coronary catheterization for acute MI in the three participating centers, 775 (11.3%) patients had a previous angiography, among which 80 (vessel n=190; 2.37±0.47 vessel/patient) were included (the sequential screening steps for clinical and analytical exclusion criteria are summarized in **Supplemental Figure 4)**. Clinical characteristics of the selected patients are summarized in **Table 1**. At the time of the MI, mean age of patients was 70.3±12.7 years, 28.7% were female and 76.3% were on Aspirin and 90.0% on statins. Non-ST elevation myocardial infarction (NSTEMI) and STEMI were reported in 65% and 35% of the studied patients, respectively. Percutaneous coronary intervention was performed in 97.5% (78/80) of cases. The culprit lesion was located in the LAD in 43.8% of cases, in the LCX in 28.7% of cases and in the RCA in 27.5% of cases. Median time between baseline and index angiography was 25.9 (IQR 21.9-29.8) months. The angiography-based analysis of QCA, vFFR and WSS was equally feasible in 98.9% of vessels (188 vessels, of which FCL n=80, NCL n=108).

Anatomical and functional parameters and risk for subsequent myocardial infarction

Percent AS was significantly higher in the FCL group (63.1±12.4 vs. 55.8±12.5, $p<0.001$). Distal vFFR was lower in FCL compared to NCL (0.84 (IQR 0.75-0.90) vs. 0.86 (IQR 0.82-0.92), $p=0.009$); whereas ΔvFFR was higher in FCL compared to NCL (0.08 (IQR 0.04-0.13) vs. 0.05 (IQR 0.03-0.08), $p=0.002$) with a pressure drop across the lesion of 14.5 (IQR 9.0-22.5) mmHg in FCL vs. 12.0 (IQR 8.0-16.0) mmHg in NCL ($p=0.012$; **Table 2**). %AS and ΔvFFR emerged as moderate independent predictors for MI (%AS AUC 0.65, 95%CI

0.57-0.73, $p<0.001$ and ΔvFFR AUC 0.63, 95%CI 0.55-0.71, $p<0.001$), with best cut-off values derived from ROC curves analysis equal to 55.5% for %AS and 0.05 for ΔvFFR (**Supplemental Table 2)**.

Wall shear stress descriptors and risk for future myocardial infarction

On average, the computational time per clinical CFD-based WSS analysis was 10.8±1.41 min.

Differences in the distribution of WSS-based quantities between the FCL and NCL groups at the lesion level are reported in **Supplemental Figure 5**, while comparison of the heat maps of WSS-based quantities as obtained from the two CFD approaches are presented in **Supplemental Figure 6**. OSI average values were a scale factor of ten lower than the OSI upper bound value (by construction, $0 \leq OSI \leq 0.50$), and on average approximated zero. For this reason, OSI was not considered in the further analyses.

Results of the univariate analysis are reported in **Supplemental Table 2**. Both TAWSS and TSVI values were significantly higher in the FCL group at the level of the lesion segment (4.58 Pa in FCL vs. 3.38 Pa in NCL, $p=0.01$ and 89.00 m^{-1} in FCL vs 49.10 m^{-1} in NCL, $p<0.001$, respectively, **Supplemental Table 3**). The ROC curves analysis of TAWSS and TSVI, evaluated at the lesion level, showed moderate and high predictive capacity for MI (TAWSS AUC 0.61, 95%CI 0.53-0.69, $p=0.003$; TSVI AUC 0.77, 95%CI 0.71-0.84, $p<0.001$), respectively. The best cut-off values were to 5.01 Pa and 40.50 m^{-1} for TAWSS and TSVI, respectively. The capacity of TSVI to predict the clinical outcome MI was markedly higher than TAWSS (**Figure 2** and **Supplemental Figure 7**). This was also confirmed when evaluating predictive capacity separately for NSTEMI (TAWSS AUC 0.63, 95%CI 0.53-0.73,

p=0.007; TSVI AUC 0.74, 95%CI 0.66-0.83, *p*<0.001) and STEMI (TAWSS AUC 0.58, 95%CI 0.44-0.72, *p*=0.131; TSVI AUC 0.83, 95%CI 0.73-0.93, *p*<0.001).

The reproducibility of the CFD-based WSS analyses quantities was excellent (TAWSS ICC 0.98, 95%CI 0.95-0.99 and TSVI ICC 0.96, 95%CI 0.91-0.98), **Supplemental Figure 8**).

Multivariable predictive models for myocardial infarction

Compared with the anatomical model with %AS (model 1), the inclusion of ΔvFFR (model 2), while not adding predictive capacity (model 1: AUC 0.65, 95%CI 0.57-0.73; model 2: AUC 0.66, 95%CI 0.58-0.74; *p*=0.460), led to a significant improvement in the reclassification and in the discrimination capacity (NRI 0.53, 95%CI 0.25-0.80, *p*<0.001; relative IDI 0.03, 95%CI 0.001-0.05, *p*=0.020) for the identification of lesions culprit of subsequent MI. Similarly, the addition of TAWSS (model 3 based on TAWSS) led to a non-significant increase in the predictive capacity of the model for detecting FCL (model 2: AUC 0.66, 95%CI 0.58-0.74; model 3 based on TAWSS: AUC 0.69, 95%CI 0.61-0.76; *p*=0.099) with a significant improvement in the reclassification capacity and discriminatory gain (NRI 0.45, 95%CI 0.21-0.69, *p*<0.001; relative IDI 0.04, 95%CI 0.01-0.07, *p*=0.008). On the contrary, the addition of TSVI to the anatomical and pressure model, led to a significant increase in predictive capacity for MI (model 2: AUC 0.66, 95%CI 0.58-0.74; model 3 based on TSVI: AUC 0.77, 95%CI 0.70-0.84; *p*<0.001; **Supplemental Figure 9** and **Supplemental Table 4**) with incremental reclassification and discriminatory capacity (NRI 1.04, 95%CI 0.81-1.27, *p*<0.001; relative IDI 0.22, 95%CI 0.16-0.27, *p*<0.001; **Supplemental Tables 5** and **6**).

Time-to-event analysis

Event-free probabilities were investigated for %AS, ΔvFFR, TAWSS and TSVI (**Figure 3, Supplemental Figures 10** and **11)**. The single strongest predictor of MI at the lesion level was TSVI (HR 5.11, 95%CI 2.70-9.68, p<0.001; **Supplemental Table 7**). An increment of TSVI of 100 m^{-1} was associated with six-fold increased odds for a future MI (OR 5.97, 95%CI 2.94-13.5; **Supplemental Figure 12**).

Discussion

The present study proved that a comprehensive approach based on a novel 3DQCA software is able to identify lesions culprit of future MI. The main findings of the study can be summarized as follows: (i) a 3DQCA-based software was able to provide in few minutes reliable WSS-based quantities from CFD simulations from standard angiographic images; ii) FCL had higher area stenoses, higher pressure gradients, and higher TAWSS and TSVI values than the control lesions; (iii) a model integrating anatomical, pressure and WSS descriptors showed improved discriminatory and reclassification capacity in identifying lesions culprit of future MI compared with a model based on anatomy and pressure gradients alone; (iv) a recently introduced WSS-based descriptor measuring the variability of the contraction/expansion action exerted by the WSS on the endothelium along the cardiac cycle, TSVI, [19] exhibited strong predictive capacity for future MI.

Studies based on intravascular imaging led to the identification of several markers of plaque vulnerability.[20, 21] Nevertheless, the vast majority of these 'high-risk plaques' become quiescent over time, thus challenging the vulnerable plaque concept.[20] On the other hand, since mild lesions outnumber severe stenoses, a sizable proportion of MI occurs at the site of mild lesions.[19] Using coronary computed tomography angiography (CCTA) the EMERALD study demonstrated the added value of the integration of hemodynamic features with plaque characteristic to identify lesions prone to rupture.[22] Pursuing a similar aim, the present study combined angiographic information with translesional pressure and WSS-based quantities. Lesions were classified as culprit and non-culprit according to an overt clinical event, and NCL served as internal control, thus accounting for the intrinsic biological variability. In contrast to

previous studies, the culprit criterion referred to a clinically relevant endpoint (i.e. MI), thus minimizing biases related to softer endpoints, such as anatomical plaque progression or target vessel revascularization.[23, 24]

Applicability and reliability of CFD simulations based on conventional angiography

Based on recent studies confirming the reliability of angiographically-derived WSS,[25] the present work nurtured from the combination of conventional coronary angiography and CFD algorithms, allowing for a multidimensional lesion evaluation. Despite this complexity, a remarkable clinical implication of the present study is that all analyses were obtained by a clinician in 10.8±1.41 minutes from conventional angiography using a standard computer. Hence, the methodological approach offered in the present study brings WSS and derived quantities closer to the clinical environment, where otherwise CFD simulations require substantial computational efforts, and in most cases mandate the support of experts.

To further legitimate the clinical application of the investigated clinical CFD approach, the reliability for WSS calculation was tested against simulations with higher resolution and numerical robustness carried out by experts in computational hemodynamics. The reliability of the clinical CFD approach was tested in terms of statistical significance rather than as reproducibility at the single-node level of computational grids. The comparison of the heat maps of WSS-based quantities as obtained from the two CFD approaches (**Supplemental Figure 6**) highlighted that the clinical CFD is adequately robust to replicate the results obtained using expert CFD, in terms of MI predictivity. The clinical CFD allowed for a WSS calculation in shorter times without substantial loss in WSS predictive strength of MI.

Inclusion of computational hemodynamics for MI prediction

Anatomical lesion severity and translesional vFFR had a significant albeit modest capacity of detecting lesions culprit of future MI (**Supplemental table 5**). For this reason, this study also investigated the action of shear forces at the blood-endothelium interface. Previous studies have shown that low TAWSS (<1.50 Pa) was associated with endothelial dysfunction and plaque progression,[6] while high TAWSS (>4.71 Pa) in the proximal segments of the atherosclerotic plaque was predictive of plaque disruption and MI.[7] More recently, a maximal TAWSS above 4.95 Pa over 3 mm vascular segment independently predicted adverse cardiovascular events requiring revascularization.[25] A significant association between TAWSS and the occurrence of MI was confirmed also in the present study (p=0.011), and in line with previous findings TAWSS significantly predicted MI, albeit weakly (TAWSS AUC 0.61, 95%CI 0.53-0.69, p=0.003). Moreover, the TAWSS cutoff (i.e. 5.01 Pa) supports previous reports.[7] However, in contrast with the EMERALD study and the FAME 2 WSS sub-analysis,[7, 22] the present study cohort had a lower functional lesion severity as depicted by the proportion of hemodynamically significant lesions (19.7% vs. 49.0% vs. 100.0% in the current study, EMERALD and FAME 2, respectively). Finally, vessels with borderline FFR values (0.81-0.85) and lesions with %AS <58% and maximum TAWSS <7.69 Pa had a long-term prevalence of lesion-oriented events below 6%.[26] Our study confirmed similar predictive cutoffs for both %AS (55.5%) and maximum TAWSS (7.30 Pa).

These findings highlight the potential usefulness of the current approach in stratifying mild lesions, hence tailoring preventive therapeutic strategies in patients without hemodynamically significant lesions.

Emerging role of TSVI

WSS topological skeleton features identify blood flow stagnation, recirculation and separation regions,[27] previously identified as flow disturbances promoting atherosclerosis.[12] Among WSS topological skeleton features, TSVI was initially associated with development of long-term re-stenosis after carotid endarterectomy in humans[8]. Recently, TSVI has been linked with early atherosclerotic changes in coronary arteries in preclinical swine models.[10] Of note, high TSVI not only co-localized with higher wall thickness, but also predicted wall thickening longitudinally.[10]

Based on these recent findings, this is the first study investigating the link between TSVI and MI. More specifically, TSVI quantifies the variability in the contraction/expansion action exerted by the WSS on the endothelium along the cardiac cycle. [8, 17] Translating this into mechanistic implications, high WSS contraction/expansion variability, inducing endothelial intra- and intercell tension variability, might promote shrinking/widening of cellular gaps,[27] fibrous cap fragility, accelerated disease progression, up to plaque rupture with impact on clinical outcomes.[4] This hypothesis, although warranting further investigation, is grounded on the predictive capacity for MI of TSVI at the lesion level and downstream of the lesion in the present study (**Supplemental Table 2**). Moreover, among 60 lesions with %AS, ΔvFFR and TSVI above the threshold values, 45 (75%) evolved into a MI (**Supplemental Figure 11**). This enhanced discrimination for plaques vulnerable to rupture or, conversely, prone to senescence

may provide the foundations for future clinical studies addressing different therapeutics strategies in this subgroup of patients. Of note, the best predictive performance was achieved by TSVI in predicting STEMI at 5 years (AUC 0.83, 95%CI 0.73-0.93, $p<0.001$).

Taken together with the previous evidences current results support the role of the WSS contraction/expansion action along the cardiac cycle in promoting biological events, including plaque formation, progression[8, 17] and, ultimately, destabilization. However, TSVI-associated changes in plaque characteristic remains to be elucidated.

Limitations

This study has several limitations. First, the small number of patients included in the final analysis. While explained by selection criteria of the retrospective screening, selection biases cannot be excluded. Second, the retrospective study design limited our ability of controlling for potential confounding factors, e.g. administration of intracoronary nitroglycerin before image acquisition. Third, no information on plaque burden or composition are available. Fourth, the uncertainty and the level of idealization inherent in the 3D reconstruction and the CFD modelling might influence the considered WSS-based descriptors. In particular, the lack of personalized flow measurements and the assumptions made to manage the inflow boundary conditions could affect the WSS estimation. However, the use of generic Doppler velocity curves scaled to fit patient-specific inlet cross-section diameter was previously validated in vessels presenting luminal cross sectional area reduction < 50%.[28] Moreover, in ongoing analyses on diseased coronary arteries with available Doppler and frame count data, TSVI resulted only modestly affected by the adoption of the boundary conditions applied in the present study. Analytically, a possible explanation for this can be found in the use of the normalized WSS vector in TSVI (see Eq.1).

Conclusions

The present study demonstrated (i) the value of CFD derived from conventional coronary angiography and performed by clinicians and (ii) the capability of WSS-based quantities to detect lesions culprit for future MI.

Although angiography-derived anatomical lesion severity and pressure drop along the vessel showed capacity in identifying coronary lesions leading to MI, the extension of the functional evaluation to include angiographic derived endothelial shear stress features – TAWSS and TSVI – improved the predictive capacity for MI. TAWSS, the most common WSS-based descriptor, was able to identify culprit lesions of a future MI, but with a modest predictive capacity. In contrast, high TSVI showed to portray a five-fold increase in the risk prediction for MI. Further clinical trials are required to translate these concepts into clinical practice.

Conflict of interest

Sources of Funding – Dr. Sonck and Dr. Munhoz reports receiving a research grant from the CardioPath PhD program.

Disclosures – Dr. Collet reports receiving research grants from Biosensors, Heart Flow Inc., ShockWave Medical, Pie Medical Imaging, SIEMENS, GE, Medis Medical Imaging and Abbott Vascular; and consultancy fees from Opsens, Boston Scientific, Medyria, HeartFlow Inc. and Philips Volcano; Dr. De Bruyne discloses institutional consulting fees from Abbott Vascular and Boston Scientific and equities in Philips, Siemens, GE, Bayer, HeartFlow, Edwards Lifesciences and Ceyliad. Aben JP is an employee of Pie Medical Imaging. The remaining authors have nothing to disclose.

Authors contribution

AC, MLR. DG, CCh, UM, BDB and CC wrote the main manuscript text and prepared the figures. MP was involved in building the database and the figures. TM performed statistical analyses. All authors reviewed the manuscript.

References

1. Kok AM, Molony DS, Timmins LH, Ko YA, Boersma E, Eshtehardi P, Wentzel JJ, Samady H. The influence of multidirectional shear stress on plaque progression and composition changes in human coronary arteries. EuroIntervention 2019;**15**(8):692-699.

2. Wentzel JJ, Schuurbiers JC, Gonzalo Lopez N, Gijsen FJ, van der Giessen AG, Groen HC, Dijkstra J, Garcia-Garcia HM, Serruys PW. In vivo assessment of the relationship between shear stress and necrotic core in early and advanced coronary artery disease. EuroIntervention 2013;**9**(8):989-95; discussion 995.

3. De Bruyne B, Pijls NH, Kalesan B, Barbato E, Tonino PA, Piroth Z, Jagic N, Mobius-Winkler S, Rioufol G, Witt N, Kala P, MacCarthy P, Engstrom T, Oldroyd KG, Mavromatis K, Manoharan G, Verlee P, Frobert O, Curzen N, Johnson JB, Juni P, Fearon WF, Investigators FT. Fractional flow reserve-guided PCI versus medical therapy in stable coronary disease. N Engl J Med 2012;**367**(11):991-1001.

4. Chatzizisis YS, Coskun AU, Jonas M, Edelman ER, Feldman CL, Stone PH. Role of endothelial shear stress in the natural history of coronary atherosclerosis and vascular remodeling: molecular, cellular, and vascular behavior. J Am Coll Cardiol 2007;**49**(25):2379-93.

5. Puri R, Leong DP, Nicholls SJ, Liew GY, Nelson AJ, Carbone A, Copus B, Wong DT, Beltrame JF, Worthley SG, Worthley MI. Coronary artery wall shear stress is associated with endothelial dysfunction and expansive arterial remodelling in patients with coronary artery disease. EuroIntervention 2015;**10**(12):1440-8.

6. Kumar A, Hung OY, Piccinelli M, Eshtehardi P, Corban MT, Sternheim D, Yang B, Lefieux A, Molony DS, Thompson EW, Zeng W, Bouchi Y, Gupta S, Hosseini H, Raad M, Ko YA, Liu C, McDaniel MC, Gogas BD, Douglas JS, Quyyumi AA, Giddens DP, Veneziani A, Samady H. Low Coronary Wall Shear Stress Is Associated With Severe Endothelial Dysfunction in Patients With Nonobstructive Coronary Artery Disease. JACC Cardiovasc Interv 2018;**11**(20):2072-2080.

7. Kumar A, Thompson EW, Lefieux A, Molony DS, Davis EL, Chand N, Fournier S, Lee HS, Suh J, Sato K, Ko YA, Molloy D, Chandran K, Hosseini H, Gupta S, Milkas A, Gogas B, Chang HJ, Min JK, Fearon WF, Veneziani A, Giddens DP, King SB, 3rd, De Bruyne B, Samady H. High Coronary Shear Stress in Patients With Coronary Artery Disease Predicts Myocardial Infarction. J Am Coll Cardiol 2018;**72**(16):1926-1935.

8. Morbiducci U, Mazzi V, Domanin M, De Nisco G, Vergara C, Steinman DA, Gallo D. Wall Shear Stress Topological Skeleton Independently Predicts Long-Term Restenosis After Carotid Bifurcation Endarterectomy. Ann Biomed Eng 2020.

9. De Nisco G, Tasso P, Calo K, Mazzi V, Gallo D, Condemi F, Farzaneh S, Avril S, Morbiducci U. Deciphering ascending thoracic aortic aneurysm hemodynamics in relation to biomechanical properties. Med Eng Phys 2020;**82**:119-129.

10. Mazzi V, De Nisco G, Hoogendoorn A, Calo K, Chiastra C, Gallo D, Steinman DA, Wentzel JJ, Morbiducci U. Early Atherosclerotic Changes in Coronary Arteries are Associated with Endothelium Shear Stress Contraction/Expansion Variability. Ann Biomed Eng 2021.

11. Masdjedi K, van Zandvoort LJC, Balbi MM, Gijsen FJH, Ligthart JMR, Rutten MCM, Lemmert ME, Wilschut J, Diletti R, De Jaegere P, Zijlstra F, Van Mieghem NM, Daemen J.

Validation of 3-Dimensional Quantitative Coronary Angiography based software to calculate Fractional Flow Reserve: Fast Assessment of STenosis severity (FAST)-study. EuroIntervention 2019.

12. Gijsen F, Katagiri Y, Barlis P, Bourantas C, Collet C, Coskun U, Daemen J, Dijkstra J, Edelman E, Evans P, van der Heiden K, Hose R, Koo BK, Krams R, Marsden A, Migliavacca F, Onuma Y, Ooi A, Poon E, Samady H, Stone P, Takahashi K, Tang D, Thondapu V, Tenekecioglu E, Timmins L, Torii R, Wentzel J, Serruys P. Expert recommendations on the assessment of wall shear stress in human coronary arteries: existing methodologies, technical considerations, and clinical applications. Eur Heart J 2019;**40**(41):3421-3433.

13. Ku DN, Giddens DP, Zarins CK, Glagov S. Pulsatile flow and atherosclerosis in the human carotid bifurcation. Positive correlation between plaque location and low oscillating shear stress. Arteriosclerosis 1985;**5**(3):293-302.

14. Peiffer V, Sherwin SJ, Weinberg PD. Computation in the rabbit aorta of a new metric - the transverse wall shear stress - to quantify the multidirectional character of disturbed blood flow. J Biomech 2013;**46**(15):2651-8.

15. Morbiducci U, Gallo D, Cristofanelli S, Ponzini R, Deriu MA, Rizzo G, Steinman DA. A rational approach to defining principal axes of multidirectional wall shear stress in realistic vascular geometries, with application to the study of the influence of helical flow on wall shear stress directionality in aorta. J Biomech 2015;**48**(6):899-906.

16. Himburg HA, Grzybowski DM, Hazel AL, LaMack JA, Li XM, Friedman MH. Spatial comparison between wall shear stress measures and porcine arterial endothelial permeability. Am J Physiol Heart Circ Physiol 2004;**286**(5):H1916-22.

17. Mazzi V, Gallo D, Calo K, Najafi M, Khan MO, De Nisco G, Steinman DA, Morbiducci U. A Eulerian method to analyze wall shear stress fixed points and manifolds in cardiovascular flows. Biomech Model Mechanobiol 2020;**19**(5):1403-1423.

18. DeLong ER DDaC-PD. Comparing the Areas under Two or More Correlated Receiver Operating Characteristic Curves: A Nonparametric Approach. Biometrics 1988;**Vol. 44, No. 3 (Sep., 1988), pp. 837-845**.

19. Naghavi M, Libby P, Falk E, Casscells SW, Litovsky S, Rumberger J, Badimon JJ, Stefanadis C, Moreno P, Pasterkamp G, Fayad Z, Stone PH, Waxman S, Raggi P, Madjid M, Zarrabi A, Burke A, Yuan C, Fitzgerald PJ, Siscovick DS, de Korte CL, Aikawa M, Juhani Airaksinen KE, Assmann G, Becker CR, Chesebro JH, Farb A, Galis ZS, Jackson C, Jang IK, Koenig W, Lodder RA, March K, Demirovic J, Navab M, Priori SG, Rekhter MD, Bahr R, Grundy SM, Mehran R, Colombo A, Boerwinkle E, Ballantyne C, Insull W, Jr., Schwartz RS, Vogel R, Serruys PW, Hansson GK, Faxon DP, Kaul S, Drexler H, Greenland P, Muller JE, Virmani R, Ridker PM, Zipes DP, Shah PK, Willerson JT. From vulnerable plaque to vulnerable patient: a call for new definitions and risk assessment strategies: Part I. Circulation 2003;**108**(14):1664-72.

20. Stone GW, Maehara A, Lansky AJ, de Bruyne B, Cristea E, Mintz GS, Mehran R, McPherson J, Farhat N, Marso SP, Parise H, Templin B, White R, Zhang Z, Serruys PW, Investigators P. A prospective natural-history study of coronary atherosclerosis. N Engl J Med 2011;**364**(3):226-35.

21. Johnson TW, Raber L, Di Mario C, Bourantas CV, Jia H, Mattesini A, Gonzalo N, de la Torre Hernandez JM, Prati F, Koskinas KC, Joner M, Radu MD, Erlinge D, Regar E,

Kunadian V, Maehara A, Byrne RA, Capodanno D, Akasaka T, Wijns W, Mintz GS, Guagliumi G. Clinical use of intracoronary imaging. Part2: acute coronary syndromes, ambiguous coronary angiography findings, and guiding interventional decision-making: an expert consensus document of the European Association of Percutaneous Cardiovascular Interventions. EuroIntervention 2019;**15**(5):434-451.

22. Lee JM, Choi G, Koo BK, Hwang D, Park J, Zhang J, Kim KJ, Tong Y, Kim HJ, Grady L, Doh JH, Nam CW, Shin ES, Cho YS, Choi SY, Chun EJ, Choi JH, Norgaard BL, Christiansen EH, Niemen K, Otake H, Penicka M, de Bruyne B, Kubo T, Akasaka T, Narula J, Douglas PS, Taylor CA, Kim HS. Identification of High-Risk Plaques Destined to Cause Acute Coronary Syndrome Using Coronary Computed Tomographic Angiography and Computational Fluid Dynamics. JACC Cardiovasc Imaging 2019;**12**(6):1032-1043.

23. Stone PH, Coskun AU, Kinlay S, Popma JJ, Sonka M, Wahle A, Yeghiazarians Y, Maynard C, Kuntz RE, Feldman CL. Regions of low endothelial shear stress are the sites where coronary plaque progresses and vascular remodelling occurs in humans: an in vivo serial study. Eur Heart J 2007;**28**(6):705-10.

24. Samady H, Eshtehardi P, McDaniel MC, Suo J, Dhawan SS, Maynard C, Timmins LH, Quyyumi AA, Giddens DP. Coronary artery wall shear stress is associated with progression and transformation of atherosclerotic plaque and arterial remodeling in patients with coronary artery disease. Circulation 2011;**124**(7):779-88.

25. Bourantas CV, Zanchin T, Torii R, Serruys PW, Karagiannis A, Ramasamy A, Safi H, Coskun AU, Koning G, Onuma Y, Zanchin C, Krams R, Mathur A, Baumbach A, Mintz G, Windecker S, Lansky A, Maehara A, Stone PH, Raber L, Stone GW. Shear Stress Estimated

by Quantitative Coronary Angiography Predicts Plaques Prone to Progress and Cause Events. JACC Cardiovasc Imaging 2020;**13**(10):2206-2219.

26. Tufaro V SH, Torii R, Koo BK, Kitslaar P, Ramasamy A, Mathur A, Jones DA, Bajaj R, Erdoğan E, Lansky A, Zhang J, Konstantinou K, Little CD, Rakhit R, Karamasis GV, Baumbach A, Bourantas CV. Wall shear stress estimated by 3D-QCA can predict cardiovascular events in lesions with borderline negative fractional flow reserve. Atherosclerosis 2021(02.018).

27. Melchior B, Frangos JA. Shear-induced endothelial cell-cell junction inclination. Am J Physiol Cell Physiol 2010;**299**(3):C621-9.

28. van der Giessen AG, Groen HC, Doriot PA, de Feyter PJ, van der Steen AF, van de Vosse FN, Wentzel JJ, Gijsen FJ. The influence of boundary conditions on wall shear stress distribution in patients specific coronary trees. J Biomech 2011;**44**(6):1089-95.

Figures and legends to figures

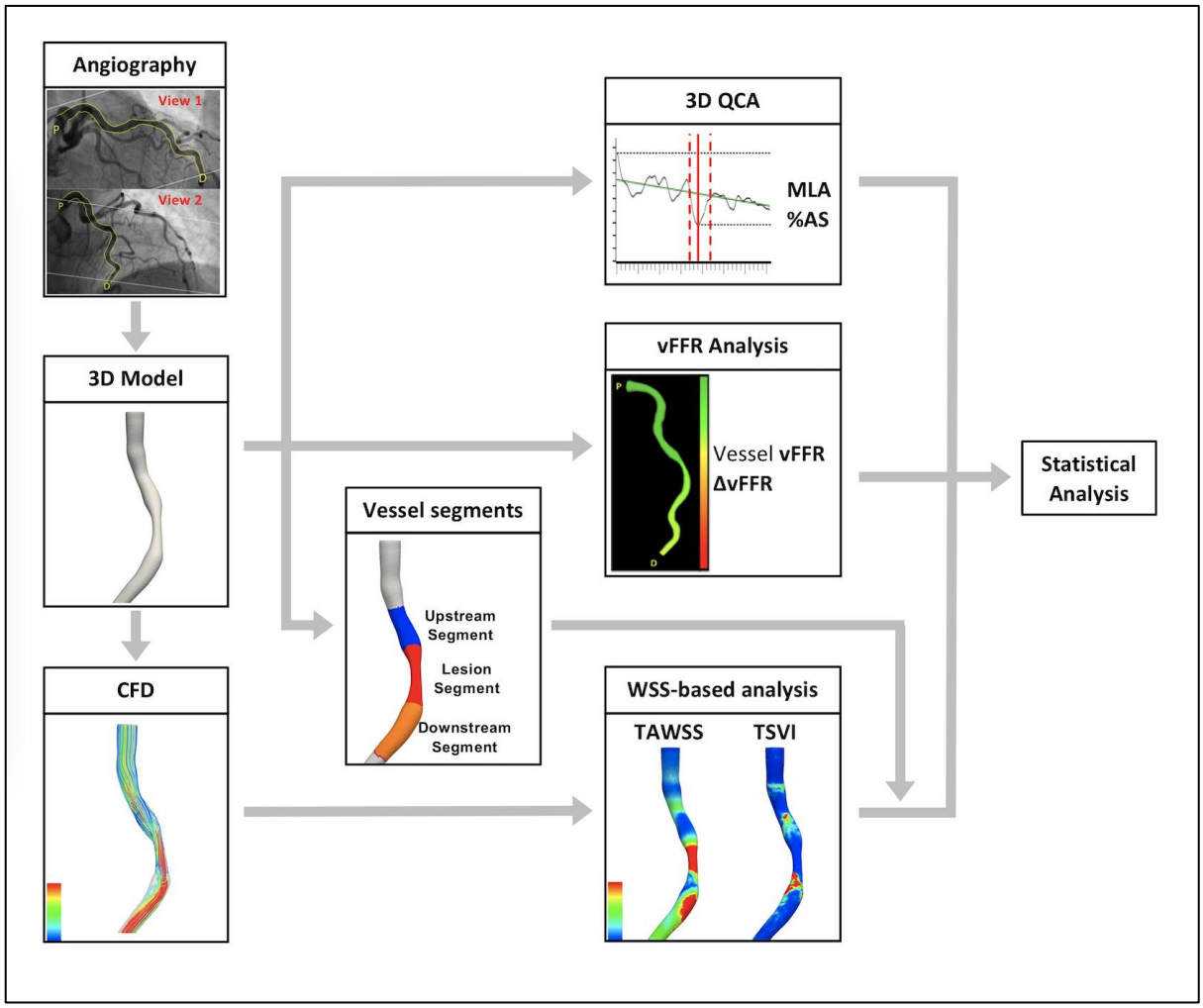


Figure 1 – Workflow of the study. The geometrical information of the three-dimensional vessel reconstruction is exploited to compute in parallel quantitative coronary angiography (QCA) analysis as well as virtual fractional flow reserve (vFFR) and computational fluid dynamic (CFD)-derived wall shear stress (WSS) simulations.

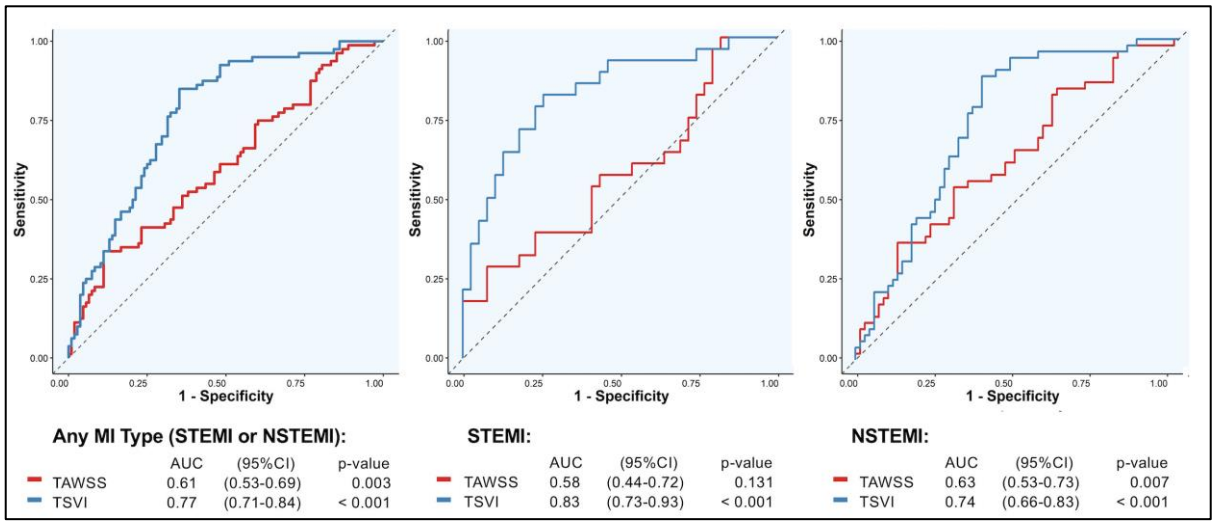


Figure 2 – Receiver operating characteristic (ROC) curves of the adopted wall shear stress descriptors. Topological shear variation index (TSVI) resulted in a good predictive capacity for any type of myocardial infarction (MI), which was significantly superior to the time-averaged wall shear stress (TAWSS). The best performance of TSVI was found in ST segment elevation myocardial infarction (STEMI).

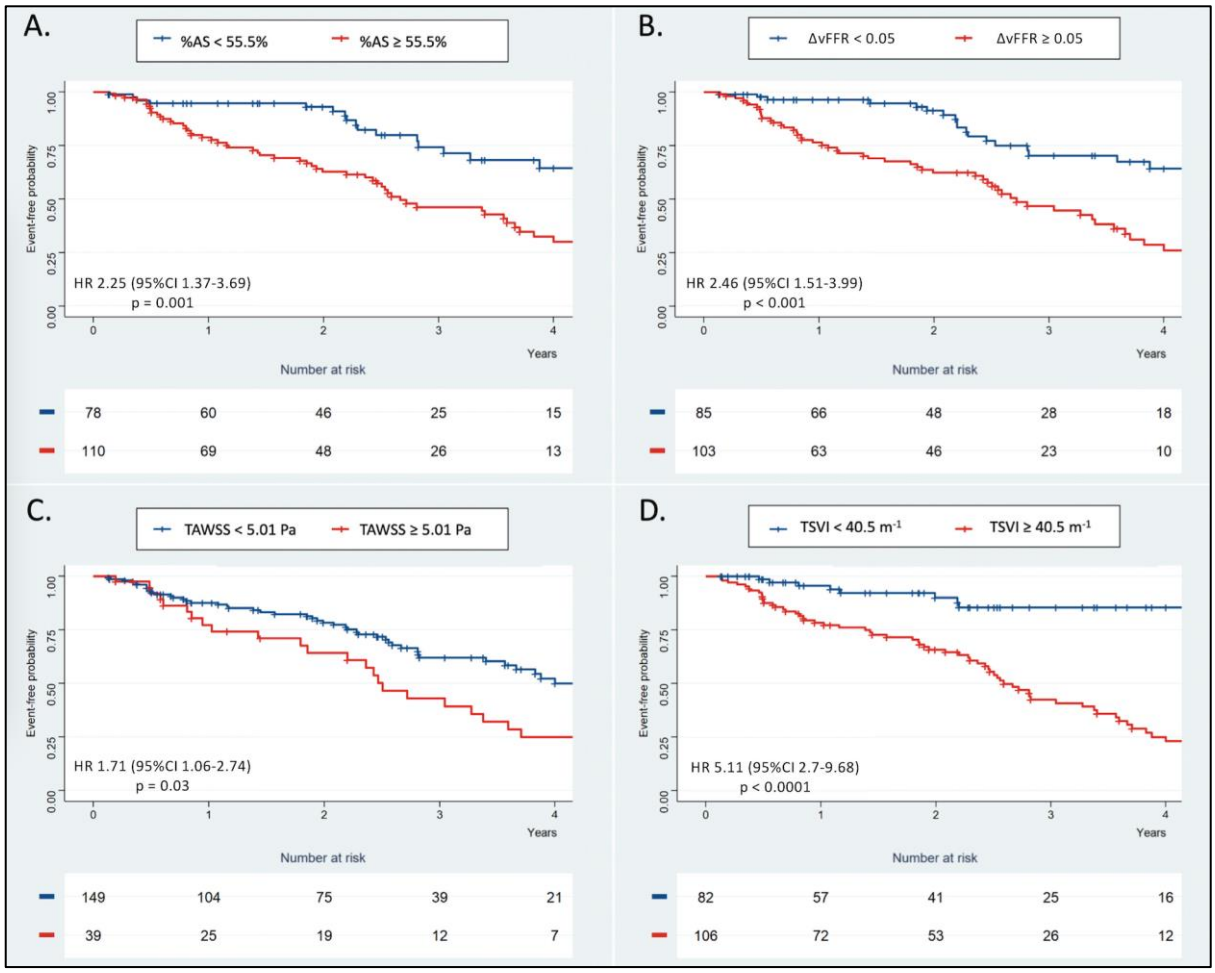


Figure 3 – Time-to-event curves. Significantly divergent Kaplan-Meier curves for future myocardial infarction are represented at 4-year follow-up for percentage area stenosis (%AS, panel A), translesional difference in virtual fractional flow reserve (ΔvFFR, panel B), lesion time-averaged wall shear stress (TAWSS, panel C) and lesion topological shear variation index (TSVI, panel D). Red and blue curves refer to values above or below the threshold values obtained from the ROC analysis, respectively. Hazard ratio (HR) refers to the whole follow-up time interval (i.e. 5 years).

1 Text tables and legends to tables

Table 1. Clinical characteristics (N= 80)	
Age, yrs	70.3 ±12.7
Female	23 (28.7%)
Type of MI - NSTEMI - STEMI	 52 (65.0%) 28 (35.0%)
Treatment - PCI - CABG - Medical	 78 (97.5) 1 (1.3%) 1 (1.3%)
Time from baseline ICA, months - 1 ICA before MI, n - ≥ 2 ICA before MI, n	 25.9 ± 17.7 67 (83.7%) 13 (16.3%)
Hypertension	61 (76.3%)
Hyperlipidaemia	63 (78.8%)
Diabetes mellitus	20 (25.0%)
- Insulin therapy	7 (8.8%)

Smoking	21(26.3%)
LVEF < 55%	18 (22.5%)
Reduced kidney function*	18 (22.5%)
Prior PCI	37 (46.3%)
Prior stroke	13 (16.3%)
Prior PVD	18 (22.5%)
Aspirin	61 (76.3%)
Statin	72 (90.0%)
P2Y12 inhibitors	15 (18.8%)

Clinical characteristics of the studied population at the time of the acute myocardial infarction (index event). Coronary artery bypass graft, CABG; Invasive coronary angiography, ICA; Left ventricle ejection fraction, LVEF; Myocardial infarction, MI; non-ST segment elevation myocardial infarction, NSTEMI; Percutaneous coronary intervention, PCI; Peripheral vascular disease, PVD; ST segment elevation myocardial infarction, STEMI. * eGFR < 60 ml/min/1.73 m2.

Table 2. Results of the quantitative coronary angiography (QCA) and the virtual fractional flow reserve (vFFR) analysis (Vessel N = 188)			
	Future culprit lesion (Vessel N = 80)	Non-culprit lesion (Vessel N = 108)	*p*-value
Vessel category			
RCA	22 (27.5%)	30 (27.8%)	0.928
LAD	35 (43.8%)	35 (32.4%)	0.184
LCX	23 (28.7%)	43 (39.8%)	0.207
Area stenosis, %	63.1±12.4	55.8±12.5	< 0.001
Diameter stenosis, %	40.2±10.6	34.3±9.66	< 0.001
Diameter stenosis			
<30%	15 (18.8%)	31 (28.7%)	0.118
≥30% and ≤50%	48 (60.0%)	72 (66.7%)	0.350
>50%	17 (21.2%)	5 (4.6%)	< 0.001
Minimal lumen area (MLA), mm^2	2.31±1.24	2.64±1.23	0.064
Minimal lumen diameter (MLD), mm	1.65±0.46	1.78±0.43	0.045
Reference vessel diameter, mm	2.78±0.63	2.74±0.62	0.668
Lesion length, mm	17.1 (IQR 11.8-26.0)	15.6 (IQR 10.3-28.3)	0.526
Distance MLA from ostium, mm	38.1 (IQR 25.2-54.3)	36.8 (IQR 23.7-55.7)	0.643
Distal pressure drop, mmHg	14.5 (IQR 9.0-22.5)	12.0 (IQR 8.0-16.0)	0.012
Distal vFFR	0.84 (IQR 0.75-0.90)	0.86 (IQR 0.82-0.92)	0.009
Distal vFFR ≤ 0.80	27 (33.8%)	10 (9.3%)	<0.001

ΔvFFR	0.08 (IQR 0.04-0.13)	0.05 (IQR 0.03-0.08)	0.002
Contour correction, %	9.5 (IQR 5.5-14.75)	10.2 (IQR 6.0-14.75)	0.486

Output of the quantitative coronary angiography (QCA) and virtual fractional flow reserve (vFFR) according to the a priori known clinical classifier (culprit or nonculprit). Interquartile range (IQR). ΔvFFR, translesional vFFR difference.